A Conserved Arginine Residue in the Pore Region of an Inward Rectifier K Channel (IRK1) as an External Barrier for Cationic Blockers

Ravshan Z. Sabirov, Tomoko Tominaga, Akiko Miwa, Yasunobu Okada, and Shigetoshi Oiki

From the Department of Cellular and Molecular Physiology, National Institute for Physiological Sciences, Okazaki 444, Japan

ABSTRACT The number, sign, and distribution of charged residues in the pore-forming H5 domain for inward-rectifying K channels (IRK1) are different from the otherwise homologous H5 domains of other voltage-gated K channels. We have mutated Arg^{148}, which is perfectly conserved in all inward rectifiers, to His in the H5 of IRK1 (Kir2.1). Channel activity was lost by the mutation, but coexpression of the mutant (R148H) along with the wild-type (WT) mRNA revealed populations of channels with reduced single-channel conductances. Long-lasting and flickery sublevels were detected exclusively for the coexpressed channels. These findings indicated that the mutant subunit formed hetero-oligomers with the WT subunit. The permeability ratio was altered by the mutation, while the selectivity sequence ($K^+ > Rb^+ > NH_4^+ >> Na^+$) was preserved. The coexpression made the IRK1 channel more sensitive to extracellular block by Mg^{2+} and Ca^{2+}, and turned this blockade from a voltage-independent to a -dependent process. The sensitivity of the mutant channels to Mg^{2+} was enhanced at higher pH and by an increased ratio of mutant:WT mRNA, suggesting that the charge on the Arg site controlled the sensitivity. The blocking rate of open channel blockers, such as Cs^+ and Ba^{2+}, was facilitated by coexpression without significant change in the steady state block. Evaluation of the electrical distance to the binding site for Mg^{2+} or Ca^{2+} and that to the barrier peak for block by Cs^+ or Ba^{2+} suggest that Arg^{148} is located between the external blocking site for Mg^{2+} or Ca^{2+} and the deeper blocking site for Cs^+ or Ba^{2+} in the IRK1 channel. It is concluded that Arg^{148} serves as a barrier to cationic blockers, keeping Mg^{2+} and Ca^{2+} out from the electric field of the membrane.

KEY WORDS: mutagenesis • Mg^{2+} block • coexpression • open channel blocker • electrical distance

INTRODUCTION

A physiologically important property of inwardly rectifying potassium channels is their very high sensitivity to cytosolic Mg^{2+} (Matsuda, 1991; Doupnik et al., 1995) that limits outward current. Carrying inward current is also important for inward rectifiers in some physiological conditions (e.g., reentry of locally accumulated K ions; see other examples in Hille, 1992). The channel faces a fairly high extracellular concentration of Mg^{2+}. External Mg^{2+} preferentially blocks the inward current (Shioya et al., 1993). In contrast to the Mg^{2+} effect from inside, the block by external Mg^{2+} is voltage independent and the sensitivity to external Mg^{2+} is very low; i.e., in the millimolar range (Biermans et al., 1987; Kell and DeFelice, 1988; Shioya et al., 1993; Elam and Lansman, 1995). This dramatic contrast in the Mg^{2+} sensitivity from inside and outside may reveal a physical picture of the inward-rectifying K (IRK)[1] pore that can be expected to be highly asymmetric.

To gain insight into the structural requirements for external Mg^{2+} sensitivity, the sequence of the H5 segment was aligned for inward rectifier and voltage-gated K^+ channels (Fig. 1). The charge distribution of the H5 region of inwardly rectifying potassium channels is quite different from those of voltage-dependent K^+ channels. The only charged residue within the H5 region of voltage-gated channels is Asp next to the conserved Gly-Tyr-Gly motif that is common to all known K^+ channels. In contrast, inward rectifiers possess one or two negatively charged Glu located near the center of H5 and one highly conserved positively charged Arg that is located at the COOH-terminal end of H5 and separated from the Gly-Tyr-Gly motif by an aromatic Phe or Tyr (Fig. 1). We focused on the conserved Arg^{148} of the IRK1 channel (Kir2.1; Kubo et al., 1993*a*; Kubo, 1996) that may face to the external environment. The "fractionally" charged residue, His, was introduced to this site (R148H).

In an attempt to clarify a physical picture of the IRK channel, electrophysiological studies were carried out by probing with cationic blockers. The results show that Arg^{148} of the IRK1 channel forms an electrostatic barrier at the external entrance of the pore and prevents block by extracellular Mg^{2+} and Ca^{2+}. Thus, the channel's high barrier to external Mg^{2+} in combination with a high affinity blocking site for internal Mg^{2+} makes it work effectively as an "inward rectifier."

Address correspondence to S. Oiki, Department of Cellular and Molecular Physiology, National Institute for Physiological Sciences, Myodaiji, Okazaki 444, Japan. Fax: 81-564-52-7913; E-mail: oiki@nips.ac.jp

[1]*Abbreviations used in this paper:* f_m, fraction of the mutant in mRNA mixture; I-V, current–voltage; IRK, inward-rectifying K; NMDG, *N*-methyl-D-glucamine; WT, wild type.

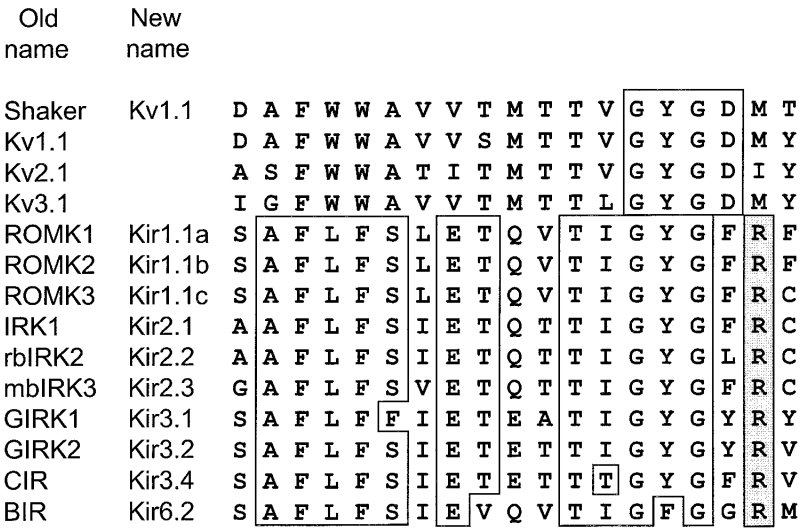

FIGURE 1. Sequence alignment of the pore region from different cloned potassium channels. *Shaker* (Kv1.1; Tempel et al., 1987), Kv1.1 (Baumann et al., 1988), Kv2.1 (Frech et al., 1989), and Kv3.1 (Yokoyama et al., 1989) encode voltage-gated K^+ channels. ROMK1 (Kir1.1a; Ho et al., 1993), ROMK2 (Kir1.1b; Zhou et al., 1994), and ROMK3 (Kir1.1c; Shuck et al., 1994) are ATP-activated weak inward rectifiers cloned from kidney. IRK1 (Kir2.1; Kubo et al., 1993*a*), rbIRK2 (Kir2.2; Koyama et al., 1994), and mbIRK3 (Kir2.3; Morishige et al., 1994) are cloned from a mouse macrophage cell line, rabbit brain, and mouse brain, respectively, and highly expressed in heart, brain, and skeletal muscle; these channels exhibit steep inward rectification. GIRK1 (Kir3.1; Kubo et al., 1993*b*), GIRK2 (Kir3.2; Lesage et al., 1994), and CIR (Kir3.4; Krapivinsky et al., 1995) are cloned from rat heart, mouse brain, and rat heart, respectively, and represent G-protein–activated inwardly rectifying K^+ channels. BIR (Kir6.2; Inagaki et al., 1995) is cloned from rat pancreatic islets and encodes inwardly rectifying K^+ channels that are inhibited by intracellular ATP. For inward rectifiers, the abbreviations that the authors originally used and "unified" names (Chandy and Gutman, 1993; Nichols and Lopatin, 1997) are given. The shaded box represents the Arg residue highly conserved in all types of inward rectifiers. The open frames enclose other conserved segments in the P-region.

METHODS

Molecular Biology

The wild-type (WT) cDNA of IRK1 was a generous gift from Dr. L.Y. Jan (University of California, San Francisco, San Francisco, CA). Site-directed mutagenesis was performed using the Sculptor in vitro mutagenesis kit (Amersham International, Little Chalfont, UK). Mutation was confirmed by dideoxy sequencing of the region containing the mutation. mRNAs were synthesized by linearization with Xho, followed by transcription with T3 polymerase using the mCAP™ mRNA capping kit (Stratagene Inc., La Jolla, CA). Transcript concentration was estimated spectrophotometrically and aliquots were stored at −80°C. Stage V and VI *Xenopus* oocytes were defolliculated by collagenase treatment (Type I, 1 mg/ml for 2–4 h; Sigma Chemical Co., St. Louis, MO) in Ca^{2+}-free Barth solution, injected with 50–150 nl ("Nanoject"; Drummond Scientific, Broomall, PA) of mRNA solution (0.5 ng/nl) and incubated at 19°C in normal Barth medium supplemented with antibiotics.

Electrophysiology

Electrophysiological measurements were made 2–10 d after mRNA injection. Whole-cell currents were recorded in oocytes with the two-microelectrode voltage clamp technique using a "bath-clamp" amplifier (CA-1; Dagan Corp., Minneapolis, MN). Oocytes were impaled with two 3-M KCl-filled micropipettes (tip resistance, 0.5–1 MΩ) that served as voltage-recording and current-injecting electrodes. Separate electrodes (Ag-AgCl electrodes; IVM, Healdsburg, CA) were used to pass the bath current and control the bath potential (two-electrode "virtual ground" circuit). The voltage-sensing electrode was placed near the outside surface of the oocyte (~1 mm). To check the series resistance error, the external potential was monitored by an additional microelectrode that was placed just above the membrane surface (<50 μm). The series resistance thus evaluated was <0.2 kΩ. Series resistance compensation was used when necessary. A grounded shield was placed between the micropipettes to reduce capacitative coupling. Another current electrode for compensating capacitative current was placed in the bath. Adjusting three time constants and phase delay provided high performance in capacitance compensation. Linear leakage currents were subtracted off-line.

Control bath solution for whole-cell recordings consisted of (mM): 90 KCl, 5 HEPES, and 0.1 EGTA, pH 7.4. Niflumic acid (200 μM) was added to block endogenous chloride currents. Mg^{2+}, Ca^{2+}, Cs^+, and Ba^{2+} were added to this solution as the chloride salts to the indicated final concentrations. The free Ba^{2+} concentration was calculated according to Oiki et al. (1994).

Bathing solution was continuously perfused at a rate of 2.5–3 ml/min through a recording chamber of 0.15 ml total volume. Junction potentials were corrected for high Mg^{2+} and Ca^{2+} solutions.

Since at a high ratio of mutant mRNA in the injecting mixture the resulting current was small in amplitude, it was necessary to eliminate the possible contribution of endogenous currents to the recording currents. The averaged currents from three parallel experiments with noninjected cells were subtracted from currents measured in injected cells. For careful analysis of current–voltage (I-V) shapes (see Fig. 2 *C*) and for selectivity measurements (see Fig. 10), oocytes were injected with a maximum amount of mRNA (up to 150 nl of 0.5 ng/nl).

Cell-attached single-channel recordings were performed on oocytes after manual removal of the vitelline envelope as described by Methfessel et al. (1986). Depolarizing bath solution consisted of (mM): 100 KCl, 10 EDTA, and 10 HEPES, pH 7.3. Patch pipettes, coated with Sylgard (Corning Glass Works, Corning, NY), were filled with the bath solution used for whole-cell measurements. Single-channel recordings were performed by an Axopatch 200A patch clamp amplifier (Axon Instruments, Foster City, CA). Capacitance transients were subtracted off-line using null traces.

Voltage protocols were generated using a 486-based computer, coupled to a TL-1 or DigiData 1200 (Axon Instruments) interface. Currents were filtered at 1 kHz and sampled at 5 kHz. Data acquisition and analysis were done using pCLAMP6 (Axon Instruments).

Experiments were performed at room temperature (23–25°C).

Data Analysis

Dose–response data for cationic block were fitted to the equation:

$$I/I_o = (I/I_o - U)/\{1 + ([X]/K_d)\} + U, \quad (1)$$

where I/I_o is the fractional current in the presence of blocker at the concentration [X], K_d is the apparent dissociation constant, and U is an unblocked fraction of current at saturating [X]. The voltage dependence of blockade was examined using the Woodhull model (Woodhull, 1973) according to the equation:

$$K_d(V) = K_d(0) \exp[-z\,\delta\,FV/RT], \quad (2)$$

where $K_d(0)$ is the apparent dissociation constant at 0 mV membrane potential, δ is the fractional electrical distance from the extracellular side, z is the valence of the blocker, and F, R, and T have their usual thermodynamic meanings.

The blocking kinetics of Ba^{2+} and Cs^+ were analyzed by fitting the time course of current to a single exponential function that is the first approximation, particularly for fast blocking kinetics. Voltage dependence of the blocking rate constants was evaluated by a rate equation in which the release rate of blocker was ignored:

$$1/\tau = k(0) \exp[-z\,\delta\,FV/RT], \quad (3)$$

where τ is the blocking time constant, and $k_{(0)}$ the rate constant at 0 mV. Rewriting the equation follows the Eyring rate equation:

$$1/\tau = A \exp[-(\Delta G^{\ddagger} + z\,\delta\,FV)/RT],$$

where $\Delta G^{\ddagger}$ is the activation energy and A is the frequency factor.

The permeability ratio P_X/P_K was determined from measurements of shifts in reversal potential (ΔE_{rev}) when 90 mM KCl in the bathing solution was replaced with 10 mM KCl and 80 mM of XCl, where X was either NMDG (*N*-methyl-D-glucamine), Na, Rb, NH_4, or Cs, according to the formula derived from the Goldman-Hodgkin-Katz equation:

$$P_X/P_K = (90 \times 10^{\Delta Erev/59} - 10)/80. \quad (4)$$

Single-channel amplitudes were measured by manually placing cursors at the open and closed channel levels.

Data from three oocytes for each measurement are presented as the mean ± SD unless otherwise noted.

RESULTS

Homomeric Channel of the Mutant R148H

No channel activity was detected using the two-electrode voltage clamp technique, even when a large amount (up to 75 ng) of the mutant R148H (Arg^{148} replaced by His) mRNA was injected into *Xenopus* oocytes. Current did not appear at low pH (pH 6.0), where the His residue should be fully charged ($n = 6$, not shown). These results suggest that Arg^{148} is crucial for channel formation or function of IRK1.

Macroscopic Current of Coinjected Oocytes

To overcome the problem of nonfunctional expression, R148H mRNA was coinjected with the WT mRNA at different ratios (hereafter referred to as f_m for the fraction of the mutant in mRNA mixture). Voltage steps from +40 to −140 mV were applied from the holding potential of −30 mV. Recorded currents were small in amplitude when mutant mRNA was coinjected with that of WT (Fig. 2 *A*). The current amplitude decreased progressively as the ratio of mutant mRNA coinjected was increased (Fig. 2 *B*), while the total amount of injected mRNA was kept constant. Instantaneous current–voltage relationships in the coexpressed oocytes (Fig. 2 *C*) showed inward rectification that was similar to that of the WT IRK1 channel. However, the chord conductance–voltage (G-V) curves normalized at −140 mV showed a slight difference in shape between WT and mutant channels (Fig. 2 *D*), suggesting inhomogeneity in the coexpressed channels.

Single-Channel Current for Homo- and Hetero-Oligomer

Fig. 3 *A* shows representative single-channel traces recorded from *Xenopus* oocytes under the cell-attached patch-clamp configuration in depolarizing bath solution (see METHODS). Oocytes were injected with WT mRNA (Fig. 3 *A, left*) or a mixture of mRNA with a ratio of R148H:WT = 1/1 ($f_m = 0.5$; Fig. 3 *A, middle* and *right*). The prominent difference in the single-channel properties was that heterogeneous channels with smaller unitary amplitude (for example, 25.2 ± 0.4 pS and 14.3 ± 0.5 pS for *middle* and *right*, respectively) appeared in the coinjected oocytes. The inward-rectifying property was not changed significantly by the mutation, as seen on the I-V curves (Fig. 3 *B*).

The distribution of the unitary amplitudes obtained from different patches and different oocytes are shown as a histogram (Fig. 3 *C*). For WT IRK1 channels, a single peak with a mean unitary amplitude of −2.9 ± 0.2 pA at −100 mV was observed (Fig. 3 *C, top*). For the channels from coinjected oocytes (the R148H/WT ratio of 1:1; $f_m = 0.5$), the data from all of our single channel recordings obtained from >60 patches (>40 oocytes) were combined into a histogram (Fig. 3 *C, bottom*). The histogram, unlike the pure WT channel, displays additional peaks on current amplitude. No single channel current with unitary amplitude higher than that of the WT channel was observed.

From these observations, we conclude that the mutant channel protein was expressed on the plasma membrane of the oocytes and was able to make complexes with the WT protein to form multiple hetero-oligomeric channels with smaller single-channel conductances. Hereafter, we will use the term "hybrid channels" to refer to the channels produced by coexpression.

Effect of R148H Mutation on Mg^{2+} Blockade

In Fig. 4 *A*, the effects of external Mg^{2+} on whole-cell IRK1 currents are shown. Block by Mg^{2+} was largely in-

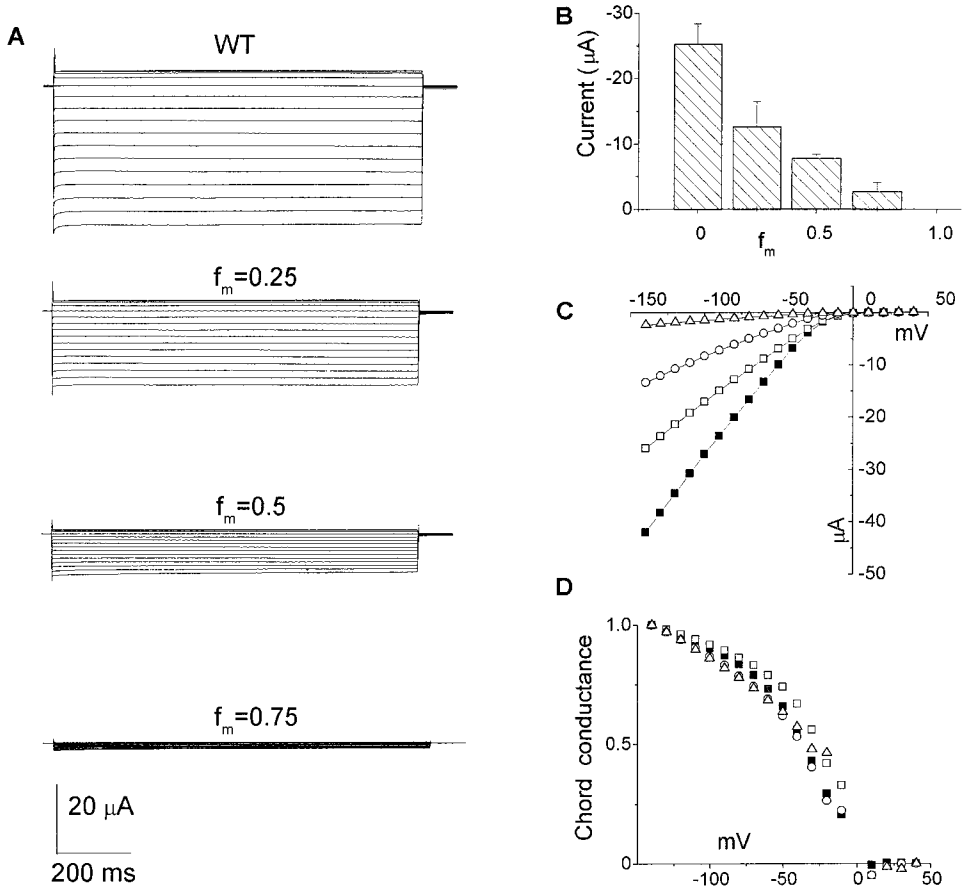

FIGURE 2. Macroscopic currents recorded from *Xenopus* oocytes injected with mRNA of the wild-type (WT), and mixture of WT and the R148H mutant at different ratios. (*A*) Representative current traces. Currents were recorded by applying steps of 1,000-ms duration from +40 to −140 mV in 10-mV decrements. Holding potential was −30 mV. (*B*) Current amplitude at −100 mV as a function of fractional R148H content in mRNA mixture. (*C*) Representative instantaneous I-V curves of the data in *A*. (*D*) The chord conductances normalized at −140 mV as a function of voltage. ■, WT; □, f_m = 0.25; ○, f_m = 0.5; △, f_m = 0.75.

stantaneous, with little effect on slow inactivation, and thus only instantaneous I-V curves are shown in Fig. 4 *B*. For both WT and mutant, the current was depressed progressively as external Mg^{2+} was increased. In Fig. 4 *C*, the concentration dependency of the relative current amplitude at −140 mV is shown. Coexpression with R148H increased the Mg^{2+} sensitivity of the K^+ currents. As the mutant:WT ratio was increased, the apparent K_d that were evaluated from Fig. 4 *C* decreased progressively from 4.4 mM for WT to 1.3 mM for hybrid channels of f_m = 0.75 (see legend to Fig. 4 *C*). For the WT channel, 31% of the current remained unblocked at saturating concentrations of Mg^{2+}. The unblocked fraction also decreased progressively as the mutant ratio was increased (5% for f_m = 0.75; see legend to Fig. 4 *C*).

Fig. 4 *D* shows representative single-channel traces recorded in the cell-attached configuration with patch pipettes containing 5 mM Mg^{2+}. The single-channel conductance was depressed significantly for the WT channel (12.8 ± 0.2 pS) in the presence of 5 mM external Mg^{2+} compared with that in the absence of external Mg^{2+} (29 pS; Fig. 3). For coinjected oocytes, no single-channel current of higher unitary amplitude than the WT channel was observed under Mg^{2+}-containing conditions. The most frequently observed hybrid channels had a single-channel conductance of 5.1 ± 0.2 pS (f_m = 0.5; Fig. 4 *D, right*). Flickery events could not be detected in either WT or hybrid channels at this recording resolution (1 kHz). The gating properties of the hybrid channels looked to be similar to those of WT. Thus, the Mg^{2+} block was mainly due to a depressed single-channel conductance.

In Fig. 5 *A*, the normalized G-V curves for the macroscopic current in the presence of extracellular Mg^{2+} are shown. For the WT channel, the shape of the G-V curve was almost flat at high negative potentials (Fig. 5 *A*, ■). The apparent K_d values showed negligible voltage dependency for the WT channel (Fig. 5 *B*). This suggests that in the WT channel the Mg^{2+}-blocking site is located outside the membrane electric field. By contrast, hybrid channels were blocked by Mg^{2+} in a potential-dependent manner. The G-V curves of hybrid channels showed a rising phase in the potential region from −140 to −60 mV (Fig. 5 *A*, *open symbols* for f_m = 0.5 and 0.75). The apparent K_d values decreased as the membrane potential was hyperpolarized (Fig. 5 *B*). The voltage dependency of apparent K_d values became steeper as the mutant:WT ratio was increased. The electrical distance of the Mg^{2+} blocking site was evaluated from the voltage-dependent K_d changes using the Woodhull

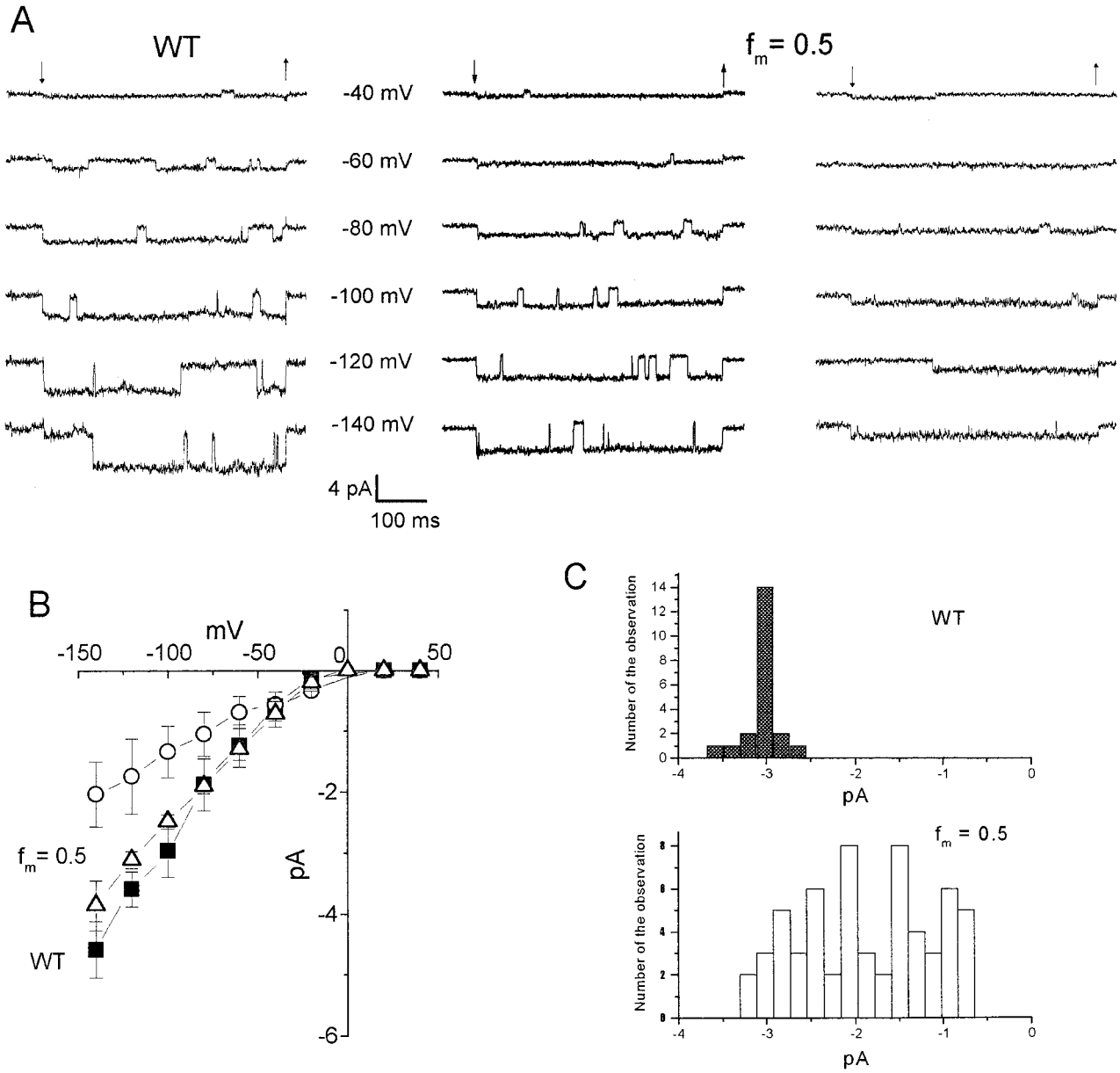

FIGURE 3. Single-channel currents of WT and R148H/WT (f_m = 0.5) hybrid channels. (*A*) Representative single-channel currents recorded from *Xenopus* oocytes injected with mRNA of WT (*left*) and the mixture of WT and the R148H mutant (f_m = 0.5; *middle* and *right*). Representative traces from channels of two different conductances are shown from coinjected oocytes. Downward and upward arrows indicate the beginning and the end of the voltage step (500 ms), respectively, from the holding potential of −30 mV. (*B*) Single-channel I-V curves for WT (■) and hybrid (○ and △) channels. (*C*) Distribution of single-channel currents for WT (*top*) and coinjected R148H/WT (f_m = 0.5) channels (*bottom*) at −100 mV obtained from different patches and oocytes (n = 21 and 60 for WT and hybrid channels, respectively).

model (Eq. 2). As the mutant:WT ratio was increased, the electrical distance progressively increased from 0.03 to 0.10 for f_m = 0.25–0.75 (Fig. 5 *C*).

Effect of pH on the Channel Activity and Mg^{2+} Blockage

To explore the basis for the higher Mg^{2+} sensitivity of the hybrid channels, we first carried out a pH titration of the His residue(s) from the extracellular side. Normalized currents ($I_{pH}/I_{pH = 8.5}$) of −140 mV at different external pH are shown in Fig. 6 *A*. The WT channel was relatively insensitive to external pH. For hybrid channels (f_m = 0.5), the current amplitude decreased significantly as the external pH was reduced, although significant currents remained at pH 6.0. The results could be well fitted by a titration curve of a single group with an apparent p*K* of 7.23 ± 0.03 at −140 mV. This value is close to the p*K* value of a His residue. Thus, the His^{148} residue appears to be located near the extracellular entrance to the pore. The apparent p*K* value implies that

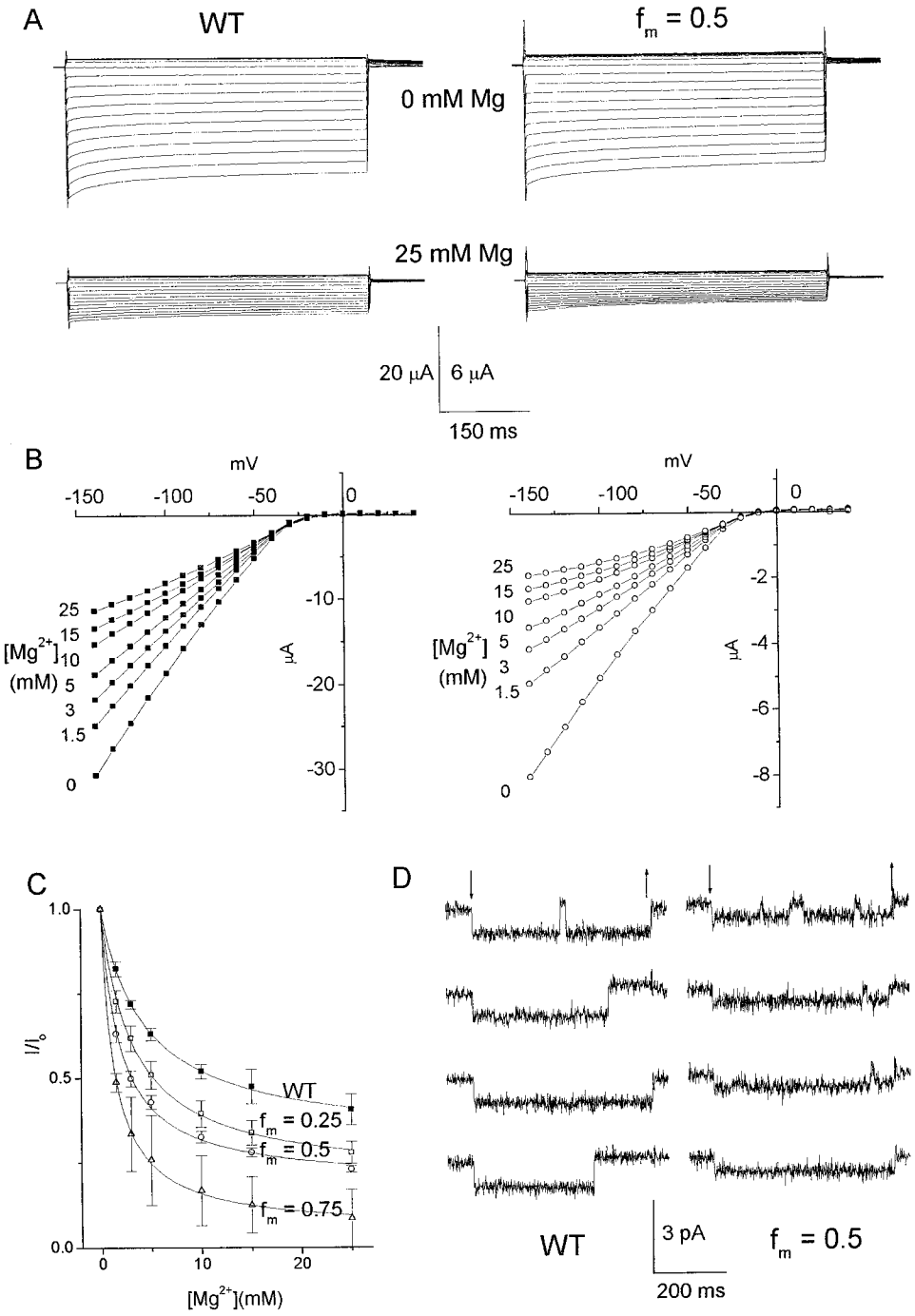

FIGURE 4. Sensitivity to external Mg^{2+} of WT and R148H/WT hybrid channels. (*A*) Representative traces of macroscopic currents recorded from *Xenopus* oocytes injected with WT (*left*) and a mixture of WT and R148H mutant mRNAs at f_m = 0.5 (*right*). The scale bar indicates 20 μA for the left traces and 6 μA for the right. Pulse protocol was the same as that of Fig. 2 *A* while the duration was 500 ms. (*B*) Instantaneous I-V curves at different concentrations of Mg^{2+} for WT and hybrid channels (f_m = 0.5). (*C*) Concentration dependency of the Mg^{2+} blockage of the fractional current at −140 mV. Curves represent fitting to Eq. 1 with K_d = 4.38 ± 0.19 mM (WT; ■), 3.21 ± 0.19 mM (f_m = 0.25; □), 1.92 ± 0.14 mM (f_m = 0.5; ○), and 1.31 ± 0.06 mM (f_m = 0.75; △). The unblocked fraction of currents was 0.31 ± 0.07 for WT, 0.20 ± 0.10 for f_m = 0.25, 0.17 ± 0.01 for f_m = 0.5, and 0.05 ± 0.01 for f_m = 0.75. (*D*) Representative traces of single-channel currents for WT (*left*) and hybrid (f_m = 0.5; *right*) channels recorded with patch pipettes filled with the bath solution containing 5 mM Mg^{2+}. Downward and upward arrows indicate the beginning and the end of the voltage step, respectively, applied repetitively to −100 mV from a holding potential of −30 mV.

a significant fraction of the His^{148} residues should be deprotonated at physiological pH.

Single-channel recordings were performed to examine protonated hybrid channels. Representative single-channel currents recorded at pH 7.06 under Mg^{2+}-free (0.1 mM EDTA in pipette solution) conditions are shown in Fig. 6 *B*. Sublevels could be detected for the hybrid channels (Fig. 6 *B, middle* and *right*) in 11 of 14 channels, whereas no sublevels were observed for the WT channel (Fig. 6 *B, left*) in all the experiments (n = 12). The same sublevels of the hybrid channels were observed less frequently at pH 7.4 (n = 5, not shown). It was surprising that we observed a long-lasting sublevel at ~50% conductance level that was rather quiet without exhibiting flickery events (Fig. 6 *B, middle*). Such long-lasting sublevels appeared exclusively for the 25 pS channel. In contrast, flickery transitions between a main level and sublevels were observed for the 20 pS channel (Fig. 6 *B, right*). The emergence of sublevels for the hybrid channels exclusively suggests that the His^{148} residue induces lower conductance substates.

The Mg^{2+} sensitivity of IRK channels was evaluated at

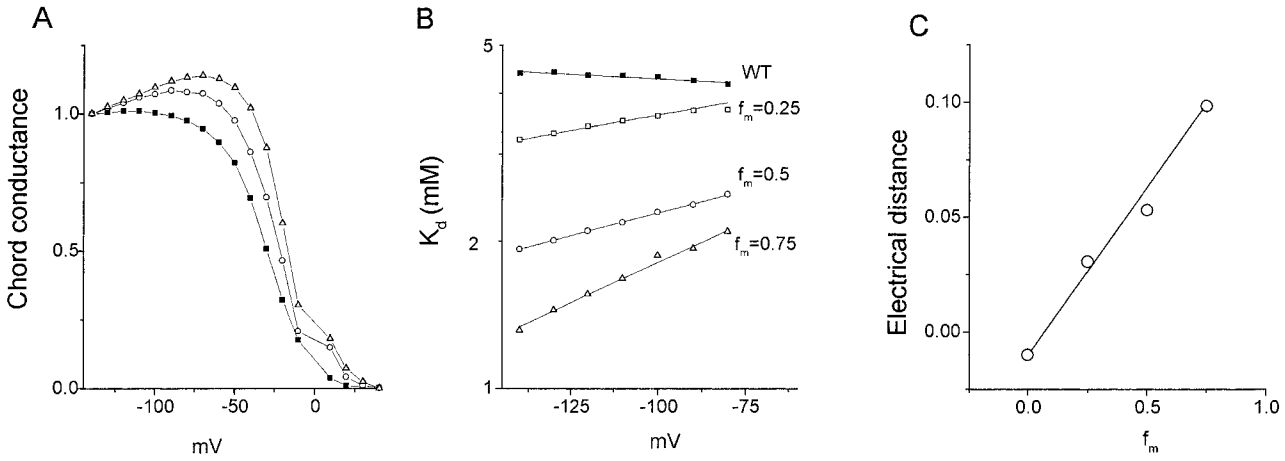

FIGURE 5. Voltage dependence of Mg^{2+} block conferred by the mutation R148H. (*A*) Chord conductances normalized to −140 mV for WT in 25 mM Mg^{2+} (■), f_m = 0.5 in 25 mM Mg^{2+} (○), f_m = 0.75 in 20 mM Mg^{2+} (△). Similar results were obtained in the presence of 5, 10, and 15 mM Mg^{2+}. (*B*) Voltage dependency of the apparent K_d of Mg^{2+} block for WT and hybrid channels. Symbols are the same as in Fig. 2. Lines represent fitting to Eq. 2 with δ plotted in *C*. $K_d(0)$ = 4.3 mM (wild type), $K_d(0)$ = 4.5 mM (fm = 0.25), $K_d(0)$ = 3.6 mM (fm = 0.5), and $K_d(0)$ = 3.8 mM (fm = 0.75). (*C*) Electrical distances for Mg^{2+} blocking as a function of the mutant ratio in mRNA mixtures.

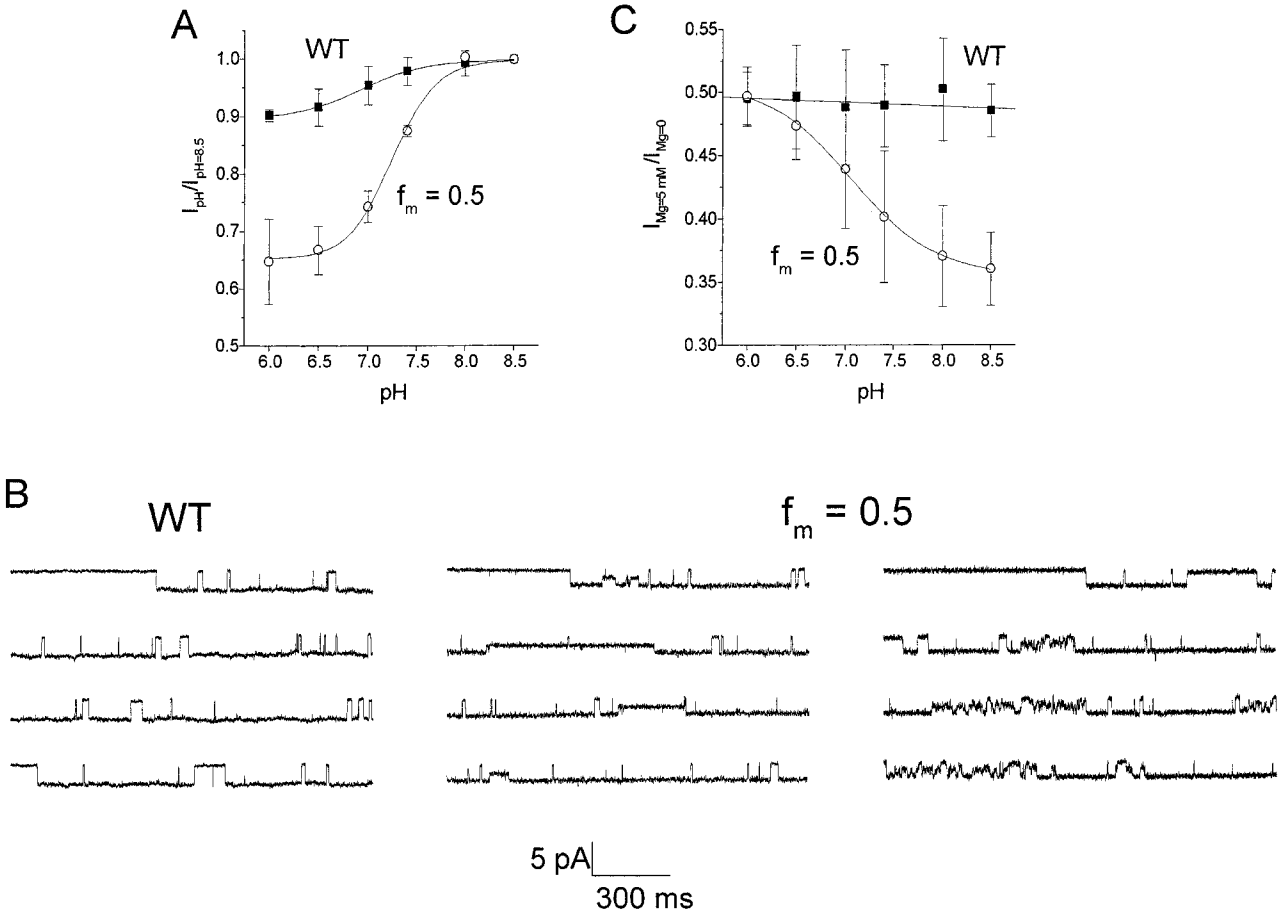

FIGURE 6. pH sensitivity conferred by the mutation, R148H. (*A*) pH dependency of the steady state current amplitude at −140 mV normalized to the control current ($I_{pH}/I_{pH\,=\,8.5}$; ■). The line fitted to the hybrid channel data represents the titration curve of a single group with pK = 7.23 ± 0.03. $[Mg^{2+}]_{bath}$ = 1 mM. (*B*) Steady state single-channel current traces, pH 7.06, recorded at −100 mV. The WT channel (30 pS) does not show sublevels. Long-lasting sublevels are shown for the 25 pS channel (*middle*) and flickering sublevels are shown for the 20 pS channel (*right*). Transition from the sublevel to the closed level was observed (for example, *B, middle second trace*). (*C*) The effect of pH on Mg^{2+} block of WT (■) and hybrid (f_m = 0.5; ○) channels. The degree of current block by 5 mM Mg^{2+} is plotted as a function of pH. Here, I_o is the current at −140 mV in Mg^{2+}-free solution and I is the current in the presence of 5 mM Mg^{2+}. The line fitted to the hybrid channel data represents the titration curve of a single group with a pK = 7.06 ± 0.03.

various pH. The fractional block by 5 mM Mg^{2+} at −140 mV ($I_{Mg=5}/I_{Mg=0}$) is shown in Fig. 6 *C*. The higher sensitivity of hybrid channels ($f_m = 0.5$) at physiological pH was augmented significantly as external pH was increased up to 8.5 (Fig. 6 *C*). When pH was decreased to 6.0, however, the difference in Mg^{2+} sensitivity between hybrid and WT channels was abolished. The apparent p*K* value thus obtained was 7.06 ± 0.03, which is very close to the apparent p*K* for the titratable current amplitude. Thus, the deprotonated His residue made the channel more sensitive to Mg^{2+} blockade, while the protonation made the hybrid channels less sensitive to Mg^{2+} with fractional blocking similar to that of the WT channel.

Effect of R148H Mutation on Ca^{2+} Blockade

Another common physiological divalent cation, Ca^{2+}, also blocked the WT IRK1 channel (Fig. 7 *A*). The apparent K_d value for Ca^{2+} measured at −140 mV was more than twice that of Mg^{2+} (see legends to Figs. 4 *C* and 7 *A*). The Ca^{2+} block of the WT IRK channel was voltage independent, as shown in Fig. 7 *C*. The effect of the mutation on Ca^{2+} block was very similar to the effect of the mutation on Mg^{2+} block. Hybrid channels were more sensitive than WT channels to Ca^{2+} and were blocked in a voltage-dependent manner, as can be seen in the G-V curves (Fig. 7 *B*) and voltage dependencies of K_d (Fig. 7 *C*). Moreover, the mutation produced the same increase in the fraction of the electrical field sensed by Ca^{2+} (up to 0.09 for $f_m = 0.75$, Fig. 7 *D*). Therefore, it is likely that the mechanisms for Ca^{2+} and Mg^{2+} block are the same.

The concentrations of divalent cations used were fairly high. However, the observed blocking effects were not due to a nonspecific increase in ionic strength, since addition of NMDG-Cl up to 180 mM produced little effect on macroscopic currents ($n = 5$, data not shown).

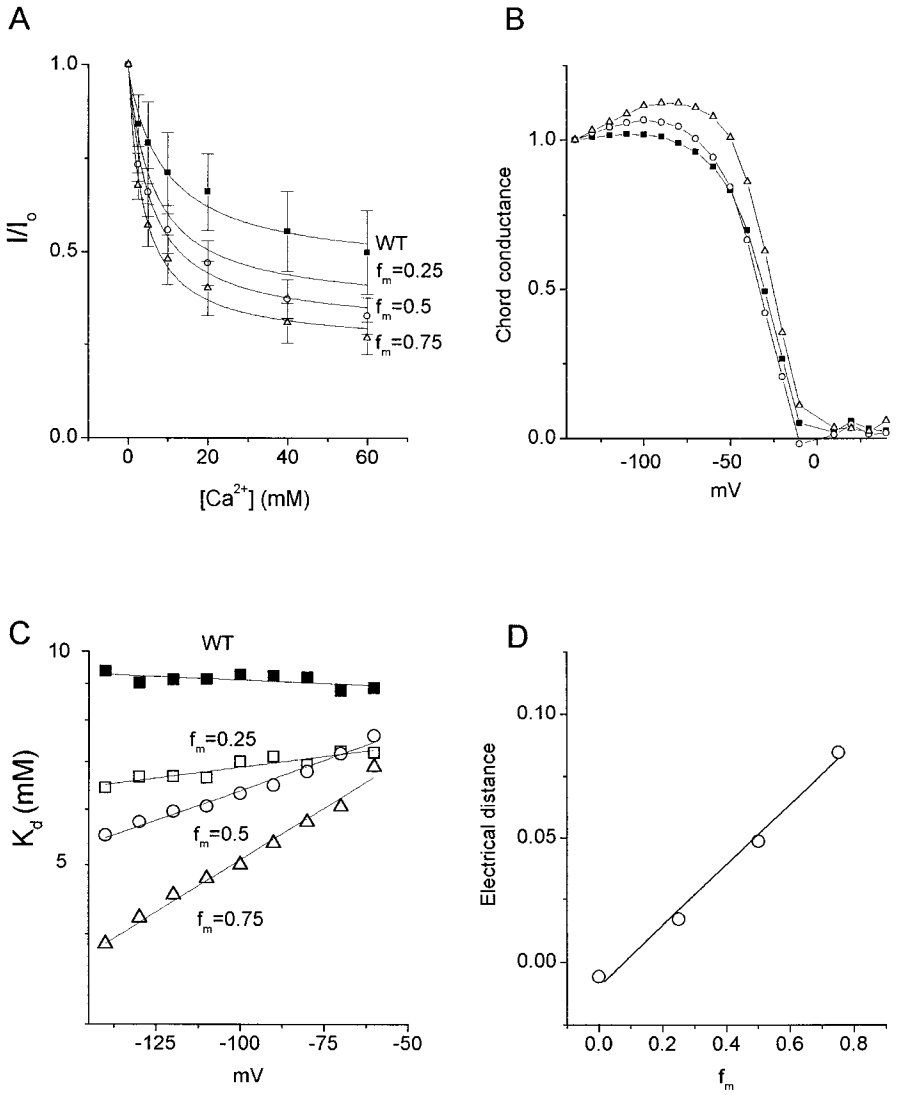

FIGURE 7. Ca^{2+} blockade of WT and hybrid channels coexpressed at different f_m. (*A*) Dose–response relationships. Curves represent fitting to Eq. 1 with K_d = 9.4 ± 2.7 mM (WT; ■), K_d = 6.4 ± 1.2 mM (f_m = 0.25; □), K_d = 5.5 ± 1.0 mM (f_m = 0.5; ○), and K_d = 3.9 ± 0.6 mM (f_m = 0.75; △). (*B*) Chord conductances normalized at −140 mV as a function of voltage for WT and 60 mM Ca^{2+} (■), f_m = 0.5 and 60 mM Ca^{2+} (○), and f_m = 0.75 and 60 mM Ca^{2+} (△). Essentially similar results were obtained in three experiments. (*C*) Voltage dependency of dissociation constants for Ca^{2+} block of WT and hybrid channels. Symbols are the same as those in Fig. 2. Lines represent fitting to Eq. 2 with δ plotted in *D*. (*D*) Electrical distances for block by Ca^{2+} as a function of mutant content in mRNA mixtures.

Effect of R148H Mutation on Cs^+ and Ba^{2+} Blockade

The potent open-channel blockers, Cs^+ and Ba^{2+}, can be used to explore, through their transient and steady state kinetics, the properties of the pore in the approach to the binding site. As illustrated in Fig. 8 *A*, the Ba^{2+} block was much slower than the Cs^+ block. For both Cs^+ and Ba^{2+}, the blocking rate was accelerated by the mutation. The current traces were fitted by a single

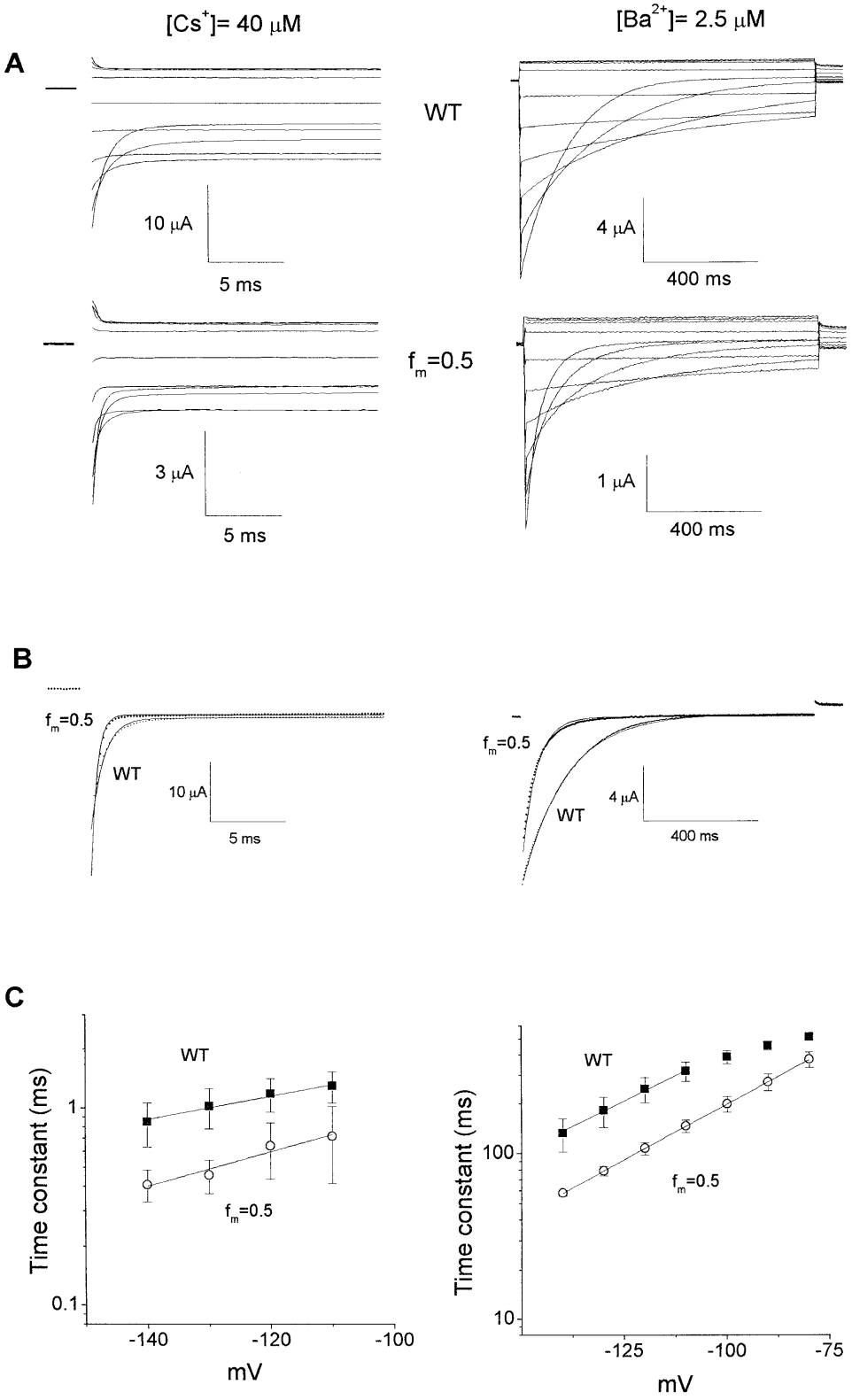

FIGURE 8. Blocking rate of Cs^+ and Ba^{2+} in WT and R148H/WT hybrid channels. (*A*) Representative current traces showing the time course of Cs^+ and Ba^{2+} block of WT (*top*) and hybrid (f_m = 0.5; *bottom*) channels. (*B*) Single-exponential fitting of blocking time course for Cs^+ (*left*) and Ba^{2+} (*right*) at −140 mV. Dotted lines correspond to fitting with time constants of 0.82 and 0.37 ms for WT and f_m = 0.5, respectively, for Cs^+ block and 149 and 57 ms for Ba^{2+} block. (*C*) Voltage dependence of the time constant for Cs^+ (*left*) and Ba^{2+} (*right*) blocking for WT (■) and hybrid (f_m = 0.5; ○) channels. Lines are fits to Eq. 3. For Cs^+ block, $k(0) = 164 \pm 32\ s^{-1}$, $\delta = 0.35 \pm 0.04$ for WT and $k(0) = 166 \pm 90\ s^{-1}$, $\delta = 0.49 \pm 0.11$ for the hybrid. For Ba^{2+} block, $k(0) = 0.13 \pm 0.01\ s^{-1}$, $\delta = 0.37 \pm 0.01$ for WT and $k(0) = 0.22 \pm 0.002\ s^{-1}$, $\delta = 0.39 \pm 0.001$ for the hybrid. The $\Delta\Delta G^{\ddagger}$ ($=\Delta G^{\ddagger}_{hybrid} - \Delta G^{\ddagger}_{WT}$) values were −0.02 *RT* for Cs^+ block and −0.47 *RT* for Ba^{2+} block.

exponential function to the first approximation (Fig. 8 *B*), where the fitting to the fast kinetics for Cs^+ blocking was an approximation due to the experimental limitations. The voltage dependency of the blocking time constants of Cs^+ and Ba^{2+} are shown in Fig. 8 *C* (*left* for Cs^+ and *right* for Ba^{2+}). In the membrane potential range tested, the blocking of hybrid channels was faster than that of WT channels.

The electrical distance to the barrier peak was calculated from the voltage dependence of the blocking time constants using the Eyring rate equation (Fig. 8 *C*; Eq. 3). In the WT channel, the electrical distances towards the barrier for Cs^+ and Ba^{2+} were similar (0.34 ± 0.04 for Cs^+ and 0.35 ± 0.02 for Ba^{2+}). Those values were only slightly affected by mutation (0.49 ± 0.08 for Cs^+ and 0.39 ± 0.02 for Ba^{2+} on hybrid f_m = 0.5). On the other hand, the height of the barrier peak was compared as a difference of the energy level between the WT channel and the mutant channels ($\Delta\Delta G^{\ddagger} = \Delta G^{\ddagger}_{hybrid} - \Delta G^{\ddagger}_{WT}$). The value of $\Delta\Delta G^{\ddagger}$ was −0.02 and −0.47 *RT* for Cs^+ and Ba^{2+} blocking, respectively. Thus, at least for the Ba^{2+} blocking, the main barrier for the blocker was depressed by the mutation without changing the position in the electric field.

In contrast to the blocking rate, the steady state blocking was not significantly effected by the mutation. The potential-dependent Cs^+ block was observed as a negative slope in the steady state I-V curves for WT channels (Fig. 9 *A*, ■). Coexpression with R148H (Fig. 9 *A*, *open symbols*; f_m = 0.5) produced little effect on I-V relationships (Fig. 9 *A*, ○). Fractional blocking as a function of Cs^+ concentration was plotted for WT and hybrid channels with different f_m (Fig. 9 *B*). The K_d values were not effected significantly by the mutation (see legend to Fig. 9 *B*). The electrical distance for steady state Cs^+ blocking was evaluated to be 1.09 ± 0.03 and was not altered by the mutation (Fig. 9 *C*). The value of the electrical distance suggests multiple ion blocking by Cs^+.

Essentially similar results were obtained for the steady state Ba^{2+} block. Similar K_d values were obtained for WT (0.15 ± 0.01 μM) and mutants (0.13 ± 0.02 μM for f_m = 0.75) for the steady state Ba^{2+} block at −140 mV. The electrical distance for the Ba^{2+} blocking site was ~0.5 for both WT (0.48 ± 0.02) and mutant channels (0.51 ± 0.04).

Effect of R148H Mutation on Ion Selectivity

The effect of the mutation on the selectivity of IRK1 channel was examined, since Arg^{148} is located close to the selectivity signature sequence. Both WT and hybrid channels did carry outward currents near the reversal potential (Fig. 10). Upon reducing the extracellular K^+ concentration from 90 to 10 mM using $NMDG^+$ or Na^+ as a substitute, the shifts in the reversal potential corresponded to the change in the Nernst potential for K^+ in both WT and hybrid (f_m = 0.75) channels (Table I). These data indicate that both WT and R148H:WT channels are practically impermeable to $NMDG^+$ and Na^+. For the Cs^+ replacement, there was no outward current, and the inward current was also very small.

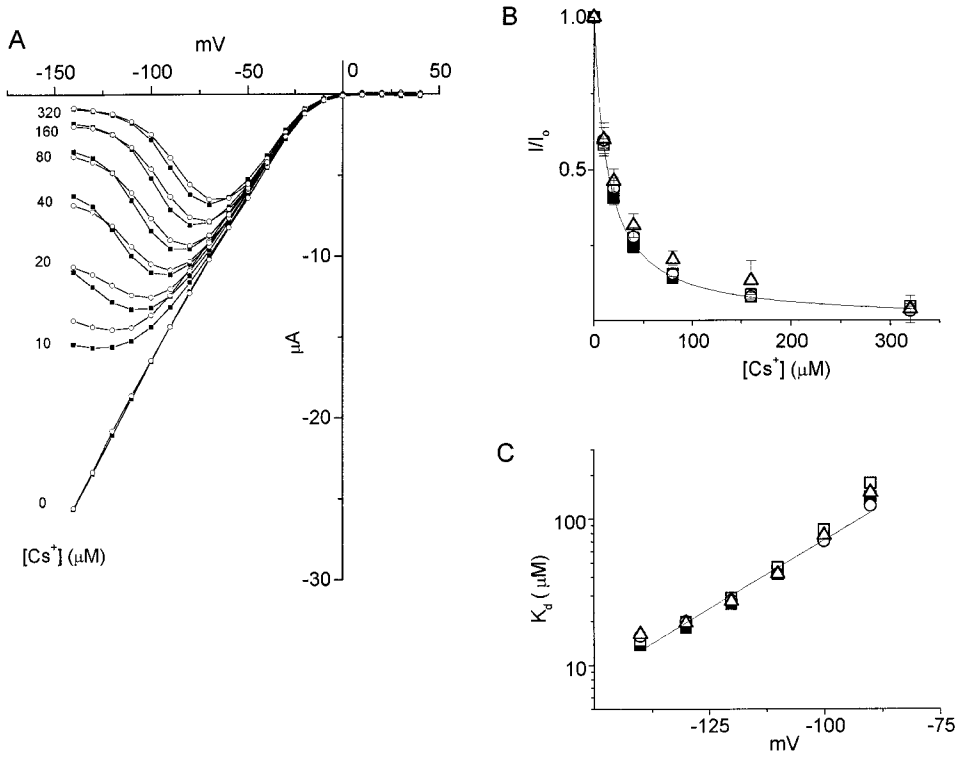

FIGURE 9. Cs^+ blocking of WT and hybrid channels. (A) Representative I-V relationships for WT (●) and hybrid (f_m = 0.5; ○) channels at different concentrations of Cs^+. Currents for hybrid channels were scaled up to match the WT current at −100 mV in the absence of blocker. (*B*) Fractional currents at −140 mV as a function of Cs^+ concentration. The curve represents fitting of the WT data to Eq. 1 with K_d = 13.7 ± 0.4 μM. 14.6 ± 0.26 μM for f_m = 0.25, 15.03 ± 0.30 μM for f_m = 0.5 and 17.24 ± 0.91 μM for f_m = 0.75.(*C*) Voltage dependence of dissociation constants. A line represents fitting of WT data to Eq. 2 with K_d (0 mV) = 5.62 ± 0.75 mM and δ = 1.09 ± 0.03. Symbols are as in Fig. 2.

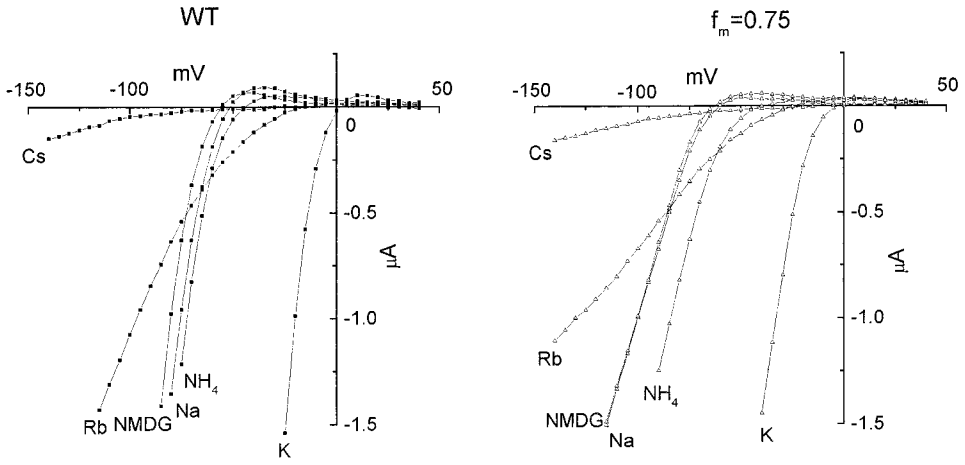

FIGURE 10. Cation selectivity of WT and R148H/WT hybrid channels. Current–voltage relationships for WT (*left*) and hybrid (f_m = 0.75; *right*) channels were observed in the presence of 10 mM KCl and 80 mM XCl, where X was either K^+, $NMDG^+$, Na^+, Rb^+, NH_4^+, or Cs^+. The holding potential was −30 mV and currents were evoked by steps from +40 to −140 mV in 5-mV increments.

Calculation of the permeability ratio for Cs^+ was not possible. By contrast, both channels were permeable to Rb^+ and NH_4^+. The outward "hump," while small in amplitude, in the I-V curve was seen in the presence of 80 mM Rb^+ or NH_4^+ ions, and the reversal potential could be determined (Table I, wild type). The permeability ratio, calculated using the Goldman-Hodgkin-Katz equation (Eq. 4), was altered by the mutation R148H (Table I, R148H:WT). The hybrid at f_m = 0.75 was still highly selective to K^+ over Na^+. The changes in Rb^+ and NH_4^+ permeabilities were significant, while the mutation did not alter the selectivity sequence $K^+ > Rb^+ > NH_4^+ >> Na^+ \cong NMDG^+$.

DISCUSSION

We have identified a residue, Arg^{148}, that is involved in protecting the IRK channel from block by extracellular divalent cations in physiological solutions. This Arg is conserved perfectly among the family of inwardly rectifying K^+ channels. The present study demonstrates that low sensitivity of the IRK channel to extracellular Mg^{2+} and Ca^{2+} is rendered by this Arg, which may serve as an electrostatic barrier for entrance of extracellular cationic blockers and keep divalent cations away from the membrane electric field.

In our experiments, the mutant molecule was coexpressed with the WT molecule, since the homo-mutant channel was nonfunctional. Recently, the tetrameric nature of the IRK channel has been revealed (Yang et al., 1995). The broad distribution of the unitary amplitude and different types of sublevels in single-channel recordings indicated that hetero-tetramer channels were formed in coinjected oocytes in the present study. Thus, the macroscopic current represented the average behavior of these heterogenous populations. On average, the number of mutant subunits in a tetramer should increase as the coinjected-mutant:WT ratio is increased (MacKinnon, 1991). Thus, the systematic changes in Mg^{2+} sensitivity observed in coexpressed oocytes such as the decreased K_d values, increased voltage sensitivity, and decreased unblocked fraction indicate an "additive" contribution of the mutant subunit, and thereby the His residues, to Mg^{2+} sensitivity in a tetrameric channel (Durkins et al., 1993).

To examine whether the higher Mg^{2+} sensitivity introduced by His^{148} was related to the protonatable nature of the His residue, titration of the His^{148} residue was performed. The macroscopic current amplitude for the hybrid channels was depressed significantly as external pH was decreased. On the other hand, the WT channel showed little sensitivity to the external pH change, although the unitary amplitude was depressed slightly at lower pH (Sabirov et al., 1997). The apparent p*K* value (7.23) for current amplitude indicated that a significant fraction of the His^{148} residue is deprotonated at physiological pH. In single-channel recordings, we could detect sublevels exclusively for the hybrid channels, suggesting that the His^{148} residue might control distinct conductance levels. In parallel to the pH dependency of the current amplitude, the sensitivity of the His^{148} subunit containing channels to Mg^{2+} became increased when external pH was increased. The similar apparent p*K* values for the Mg^{2+} sensitivity (7.06) and the current amplitude (7.23) indicate that the deprotonated His residue rendered the channel more sensitive to Mg^{2+}. In contrast, no pH dependence

TABLE I

Ionic Selectivity of WT and R148H/WT (f_m = 0.75) Channels Estimated by the Shift of Reversal Potential (ΔE_{rev})

Cations	$NMDG^+$	Na^+	Rb^+	NH_4^+
Wild type				
ΔE_{rev} (mV)	−55.6 ± 1.9	−57.6 ± 0.9	−25.8 ± 3.1	−42.4 ± 1.3
P_X/P_K	<0.004	<0.004	0.28 ± 0.05	0.09 ± 0.01
R148H:WT (f_m = 0.75)				
ΔE_{rev} (mV)	−57.1 ± 1.6	−56.1 ± 2.6	−20.2 ± 2.3	−30.6 ± 2.6
P_X/P_K	<0.005	<0.005	0.39 ± 0.04	0.22 ± 0.04

in Mg^{2+} sensitivity was detected for the WT channel. Thus, not only the average number of the His^{148} residues on a channel but also the fraction of the deprotonated His^{148} residue should enhance Mg^{2+} sensitivity. For the WT channel, permanent charge on this site in physiological solution should prevent the Mg^{2+} blocking.

One might imagine that the deprotonated His^{148} residues form the Mg^{2+} binding site. It is less likely, however, from the following experimental observations. We found that Mg^{2+} block became voltage dependent for the mutant channels. However, $K_d(0)$ values for Mg^{2+} block evaluated by the Woodhull model (see legend to Fig 5 *B*) were similar in both WT and mutant channels. Thus, in the absence of a potential difference across the membrane, the Arg^{148} site contributes little to the affinity for Mg^{2+}, suggesting that His^{148} is not the binding site for Mg^{2+}. The blocking site for the mutant channels should exist in the membrane electric field. Why did the electrical distance increase progressively as the mutant:WT ratio was increased? The reduced electrostatic repulsion from progressively lesser positive charges on the His site may allow Mg^{2+} ions to penetrate deeper into the pore. Then where is the binding site? If a blocking ion interacts with the pore wall weakly, as expected from the low affinity, then ions might have a diffuse distribution of favorable sites. Progressive depression of the electrostatic barrier at the His site may shift the most favorable site for the low affinity blocker deeper. On the other hand, the WT channel has enough of an electrostatic barrier to exclude Mg^{2+} away from the membrane electric field.

Cs^+ and Ba^{2+} entered deeper to the pore. From the transient and steady state kinetic analyses, we demonstrated a mutational effect that exclusively facilitated the blocking rate, rather than changing the blocking affinity. For the Ba^{2+} blocking, the voltage dependence of the blocking time constant was little changed by the mutation (Fig. 8). Thus, the mutational effect can be assigned to the reduced $\Delta G^{\ddagger}$ rather than δ, where the barrier is located at ~35–39% of the distance from the external entrance to the channel. This main (rate-limiting) barrier for open channel blockers seems to be formed by the Arg residues, and the higher blocking rate for mutant channels (negative $\Delta\Delta G^{\ddagger}$ values) could be due to the reduced positive charge density introduced by less positive His. For the steady state blocking, the effect of mutation was negligible. Therefore, the Arg site did not affect the binding site of Ba^{2+} and Cs^+.

It is notable that among hetero-tetramer channels no single-channel was observed that had a higher unitary amplitude than that of the WT channel. The shape of the single-channel I-V curve was not changed significantly by the mutation, indicating that the altered potential profile for permeating K^+ was quantitative rather than qualitative. Permeating K^+ ions should experience the Arg barrier just as Ba^{2+} and Cs^+ do. However, reduction of the electrostatic barrier at the His site for Ba^{2+} did not bring about an increased single-channel conductance for K^+ permeation. Steric hindrance of the His residue might predominate for K^+ permeation.

In conclusion, our experiments demonstrate that Arg^{148} is located between the deeper blocking site for Cs^+ or Ba^{2+} and the external divalent cation binding site of IRK1 channel and forms an electrostatic barrier that keeps Mg^{2+} and Ca^{2+} out from the electric field of the pore, thereby antagonizing their potent blocking effect from the extracellular side. This barrier is rate limiting for permeating blockers, such as Ba^{2+} and Cs^+, from the extracellular solution. In series with the K^+ selectivity filter represented by the Gly-Tyr-Gly motif (Heginbotham et al., 1994), the Arg^{148} barrier modifies the selectivity of permeating ions significantly. This Arg^{148} also participates in the formation of a salt bridge.

The authors thank Dr. Lilly Y. Jan (University of California, San Francisco, San Francisco, CA) for the IRK1 clone. We also thank Dr. Richard Horn (Jefferson University, Philadelphia, PA), Dr. Andrew F. James (King's College London, London, UK), and Dr. Olaf S. Andersen (Cornell University Medical College, New York) for critical reading of the manuscript. We also thank Dr. Yoshihiro Kubo (Tokyo Metropolitan Institute for Neuroscience, Tokyo, Japan) for suggestions on IRK1 expression.

This work was supported by a Grant-in-Aid on Priority Areas of "Channel-Transporter Correlation" (07276104) from the Ministry of Education, Science, Sports and Culture of Japan.

Original version received 19 May 1997 and accepted version received 9 October 1997.

REFERENCES

Baumann, A., A. Grupe, A. Ackermann, and O. Pongs. 1988. Structure of the voltage-dependent potassium channel is highly conserved from *Drosophila* to vertebrate central nervous systems. *EMBO (Eur. Mol. Biol. Organ.) J.* 7:2457–2463.

Biermans, G., J. Vereecke, and E. Carmeliet. 1987. The mechanism of the inactivation of the inward-rectifying K current during hyperpolarizing steps in guinea-pig ventricular myocytes. *Pflügers Archiv.* 410:604–613.

Chandy, K.G., and G.A. Gutman. 1993. Nomenclature for mammalian potassium channel genes. *Trends Pharmacol. Sci.* 14:434.

Doupnik, C.A., N. Davidson, and H.A.P. Lester. 1995. The inward rectifier potassium channel family. *Curr. Opin. Neurobiol.* 5:268–277.

Durkins, J.T., L.L. Providence, R.E. Koeppe II, and O.S. Andersen.

1993. Energetics of heterodimer formation among gramicidin analogues with an NH_2-terminal addition or deletion. Consequences of missing a residue at the join in the channel. *J. Mol. Biol.* 231:1102–1121.

Elam, T.R., and J.B. Lansman. 1995. The role of Mg^{2+} in the inactivation of inwardly rectifying K^+ channels in aortic endothelial cells. *J. Gen. Physiol.* 105:463–484.

Frech, G.C., A.M. VanDongen, G. Schuster, A.M. Brown, and R.H. Joho. 1989. A novel potassium channel with delayed rectifier properties isolated from rat brain by expression cloning. *Nature.* 340:642–645.

Heginbotham, L, Z. Lu, T. Abramson, and R. MacKinnon. 1994. Mutations in the K^+ channel signature sequence. *Biophys. J.* 66: 1061–1067.

Hille, B. 1992. Ionic Channels of Excitable Membranes. 2nd ed. Sinauer Associates, Inc., Sunderland, MA. 607 pp.

Ho, K., C.G. Nichols, W.J. Lederer, J. Lytton, P.M. Vassilev, M.V. Kanazirska, and S.C. Hebert. 1993. Cloning and expression of an inwardly rectifying ATP-regulated potassium channel. *Nature.* 362:31–38.

Inagaki, N., T. Gonoi, J.P. Clement IV, N. Namba, J. Inazawa, G. Gonzalez, L. Aguilar-Bryan, S. Seino, and J. Bryan. 1995. Reconstitution of I_{KATP}: an inward rectifier subunit plus the sulfonylurea receptor. *Science.* 270:1166–1170.

Kell, M.J., and L.J. DeFelice. 1988. Surface charge near the cardiac inward-rectifier channel measured from single-channel conductance. *J. Membr. Biol.* 102:1–10.

Koyama, H., K. Morishige, N. Takahashi, J.S. Zanelli, D.N. Fass, and Y. Kurachi. 1994. Molecular cloning, functional expression and localization of a novel inward rectifier potassium channel in the rat brain. *FEBS Lett.* 341:303–307.

Krapivinsky, G., E.A. Gordon, K. Wickman, B. Velimirovic, L. Krapivinsky, and D.E. Clapham. 1995. The G-protein-gated atrial K^+ channel I_{KACh} is a heteromultimer of two inwardly rectifying K^+-channel proteins. *Nature.* 374:135–141.

Kubo, Y., T.J. Baldwin, Y.N. Jan, and L.Y. Jan. 1993*a.* Primary structure and functional expression of a mouse inward rectifier potassium channel. *Nature.* 362:127–133.

Kubo, Y., E. Reuveny, P.A. Slesinger, Y.N. Jan, and L.Y. Jan. 1993*b.* Primary structure and functional expression of a rat G-protein-coupled muscarinic potassium channel. *Nature.* 364:802–806.

Kubo, Y. 1996. Effects of extracellular cations and mutations in the pore region on the inward rectifier K^+ channel IRK1. *Receptors Channels.* 4:73–83.

Lesage, F., F. Duprat, M. Fink, E. Guillemare, T. Coppola, M. Lazdunski, and J.P. Hugnot. 1994. Cloning provides evidence for a family of inward rectifier and G-protein coupled K^+ channels in the brain. *FEBS Lett.* 353:37–42.

MacKinnon, R. 1991. Determination of the subunit stoichiometry of a voltage-activated potassium channel. *Nature.* 350:232–235.

Matsuda, H. 1991. Magnesium gating of the inwardly rectifying K^+ channel. *Annu. Rev. Physiol.* 53:289–298.

Methfessel, C., V. Witzemann, T. Takahashi, M. Mishina, S. Numa, and B. Sakmann. 1986. Patch clamp measurements on *Xenopus laevis* oocytes: currents through endogenous channels and implanted acetylcholine receptor and sodium channels. *Pflügers Archiv.* 407:577–588.

Morishige, K., N. Takahashi, A. Jahangir, M. Yamada, H. Koyama, J.S. Zanelli, and Y. Kurachi. 1994. Molecular cloning and functional expression of a novel brain-specific inward rectifier potassium channel. *FEBS Lett.* 346:251–256.

Nichols, C.G., and A.N. Lopatin. 1997. Inward rectifier potassium channels. *Annu. Rev. Physiol.* 59:171–191.

Oiki, S., T. Yamamoto, and Y. Okada. 1994. Apparent stability constants and purity of Ca-chelating agents evaluated using Ca-selective electrodes by the double-log optimization method. *Cell Calcium.* 15:209–216.

Sabirov, R.Z., Y. Okada, and S. Oiki. 1997. Two-sided action of protons on an inward rectifier K^+ channel (IRK1). *Pflügers Arch.* 433: 428–434.

Shioya, T., H. Matsuda, and A. Noma. 1993. Fast and slow blockades of the inward-rectifier K^+ channel by external divalent cations in guinea-pig cardiac myocytes. *Pflügers Archiv.* 422:427–435.

Shuck, M.E., J.H. Bock, C.W. Benjamin, T.D. Tsai, K.S. Lee, J.L. Slightom, and M.J. Bienkowski. 1994. Cloning and characterization of multiple forms of the human kidney ROMK potassium channel. *J. Biol. Chem.* 269:24261–24270.

Tempel, B.L., D.M. Papazian, T.L. Schwarz, Y.N. Jan, and L.Y. Jan. 1987. Sequence of a probable potassium channel component encoded at *Shaker* locus of *Drosophila. Science (Wash. DC).* 237:770–775.

Woodhull, A.M. 1973. Ionic blockage of sodium channels in nerve. *J. Gen. Physiol.* 61:687–708.

Yang, J., Y.N. Jan, and L.Y. Jan. 1995. Determination of the subunit stoichiometry of an inwardly rectifying potassium channel. *Neuron.* 15:1441–1447.

Yang, J., M. Yu, Y.N. Jan, and L.Y. Jan. 1997. Stabilization of ion selectivity filter by pore loop ion pairs in an inwardly rectifying potassium channel. *Proc. Natl. Acad. Sci. USA.* 94:1568–1572.

Yokoyama, S., K. Imoto, T. Kawamura, H. Higashida, N. Iwabe, T. Miyata, and S. Numa. 1989. Potassium channels from NG108-15 neuroblastoma-glioma hybrid cells. Primary structure and functional expression from cDNAs. *FEBS Lett.* 259:37–42.

Zhou, H., S.S. Tate, and L.G. Palmer. 1994. Primary structure and functional properties of an epithelial K channel. *Am. J. Physiol.* 266:C809–C824.